Microchimica Acta (2018) 185: 396
https://doi.org/10.1007/s00604-018-2934-z

ORIGINAL PAPER

Voltammetric sensing of sulfamethoxazole using a glassy carbon electrode modified with a graphitic carbon nitride and zinc oxide nanocomposite

Paramasivam Balasubramanian[1] · Ramki Settu[1] · Shen-Ming Chen[1] · Tse-Wei Chen[1,2]

Received: 9 May 2018 / Accepted: 23 July 2018 / Published online: 31 July 2018

Abstract

A voltammetric sensor is described for the determination the antibiotic sulfamethoxazole (SMZ). It is based on the use of a glassy carbon electrode (GCE) modified with a nanocomposite prepared from graphitic carbon nitride and zinc oxide (g-C_3N_4/ZnO). The nanorod-like ZnO nanostructure were synthesized sonochemically. The g-C_3N_4/ZnO nanocomposite was then prepared by mixing g-C_3N_4 with ZnO, followed by ultrasonication. The morphology and structure of the nanocomposite were characterized by X-ray diffraction, Fourier-transform infrared spectroscopy and transmission electron microscopy. Under the optimal conditions, the response of the electrode, typically measured between 0.8 and 0.9 V (vs. Ag/AgCl), increases linearly in the 20 nM to 1.1 mM SMZ concentration range, and the lower detection limit is 6.6 nM. This is better than that of many previously reported sensors for SMZ. The modified electrode is highly selective, well reproducible and maintains its activity for at least 4 weeks. It was applied to the determination of SMZ in spiked human blood serum samples in with satisfactory results.

Keywords Sulfonamide drug · Sonochemical synthesis · Electrocatalysis · High electron transfer rate · Physiological fluids

Introduction

Sulfamethoxazole (SMZ) is one of the most typical antibiotic in sulfonamide family and it has a broad spectrum of antimicrobial activity against bacteria and protozoa [1]. SMZ has been extensively used in the treatment of urinary-tract infections, pneumocystis pneumonia, chronic bronchitis, meningococcal meningitis, acute otitis, toxoplasmosis, skin and soft tissue infections [2, 3]. SMZ can offer a variety of side effects that including gastro-intestinal disturbances, hypersensitivity and variety of hematological abnormalities [1, 4]. Therefore, the search for analytical systems suitable for use in routine analyses involving pharmaceutical quality control and investigation of biological samples includes simple, high-analytical frequency, and low reagent consumption method. Several analytical methods have been reported including the spectrophotometric method [5], gas chromatography-mass spectrometry [6], Plasma protein precipitation [7], and capillary electrophoresis [8]. Most of these reported methods may offer high assay selectivity, but also were expensive, time-consuming, needed tedious procedure and using expensive instruments, there is still need for reliable and simple methods. The electrochemical methods overcome the aforementioned obstacles owing to their simplicity, rapid response, low cost, offering a high sensitivity and dynamic range comparable to other analytical method [9, 10]. There are only a few reports available on the electrochemical detection of SMZ [11–15]. To fabricate excellent sensors with chemically modified electrode, the key important thing is to seek suitable electrode modification materials with good electrical conductivity and superior electrocatalysis.

ZnO is a non-toxic, thermally stable, and electrochemically active inorganic transition metal oxide [16]. It has been considered that ZnO nanostructure is the promising material for the fabrication of efficient biosensors due to its extraordinary

Electronic supplementary material The online version of this article (https://doi.org/10.1007/s00604-018-2934-z) contains supplementary material, which is available to authorized users.

✉ Shen-Ming Chen
smchen78@ms15.hinet.net

[1] Department of Chemical Engineering and Biotechnology, National Taipei University of Technology, No.1, Section 3, Zhongxiao East Road, Taipei 106, Taiwan, Republic of China

[2] Research and Development Center for Smart Textile Technology, National Taipei University of Technology, No.1, Section 3, Zhongxiao East Road, Taipei 106, Taiwan, Republic of China

properties including electron transporting, electrochemical activities [17]. Predominantly, ZnO nanorods, nanobelts, nanotubes and nanowires are promising for electrochemical sensing owing to their sufficient high surface-to-volume ration and excellent electron transport path along the length direction [18]. There has been great interest revealed towards the synthesis of ZnO nanostructure with unique morphologies using versatile methods for sensing applications [19]. However, the sonochemical synthesis of ZnO nanorods is still not reported. Usage of ultrasonic irradiation is a simple, green, and low-cost route for the preparation blend nanocomposites (NCs). With the usage of ultrasonic, extra-ordinary reaction conditions like activation surface, high pressure, and high temperature are created for a very short time in a liquid that cannot be achieved by other methods such as mechanical or magnetic stirring [20]. Unfortunately, there is still some intrinsic properties on ZnO which will restrict its wide-scale applications [21]. In order to overcome this worries and achieve better electrocatalytic activity, ZnO combined with carbon based nanomaterials. Especially, g-C_3N_4/ZnO nanocomposites have also been reported to exhibit pronounced catalytic and electrical properties due to the excellent synergy of g-C_3N_4 and ZnO [22]. As we know, graphitic carbon nitride (g-C_3N_4), as one of the most promising catalyst, can offer high surface area, high thermal and chemical stability as well as better electrocatalytic activity [23]. It is well known that g-C_3N_4 has a conjugated p-structure and the combination of ZnO and g-C_3N_4 may be an ideal system to achieve an enhanced electron transfer process [24]. For these reason, much research attention paid on the synthesis of g-C_3N_4/ZnO composite for electrochemical sensing applications.

In this work, we report synthesis of g-C_3N_4/ZnO nanocomposite by sonochemical route and it was utilized as a novel electrochemical sensor were reported for the detection of SMZ. At first, nanorods-like ZnO nanostructure were synthesized via a sonochemical approach. Then, g-C_3N_4/ZnO nanocomposite was prepared by mixing of g-C_3N_4 and ZnO followed by ultrasonication process. The g-C_3N_4/ZnO nanocomposite showed much enhanced electrochemical activity towards the SMZ detection as compared with the single g-C_3N_4 and ZnO. Owing to the synergistic electrocatalytic activity of g-C_3N_4 and ZnO nanorods not only offer a very low limit of detection (6.6 nM) and a wide dynamic range (0.02 to 1105 μM) but also provides long term stability. Furthermore, this SMZ sensor is also proven to be suitable for the detection SMZ in physiological fluids (Scheme 1).

Experimental section

Chemicals and instrumentations

Zinc acetate dehydrate ($Zn(CH_3COO)_2 \cdot 2H_2O$), sulfamethoxazole (SMZ) ($C_{10}H_{11}N_3O_3S$), disodium hydrogen phosphate (Na_2HPO_4), dihydrogen sodium phosphate (NaH_2PO_4), sodium hydroxide (NaOH), ethylene diamine [C_2H_4 $(NH_4)_2$], and urea (NH_2CONH_2) were purchased from Sigma-Aldrich (https://www.sigmaaldrich.com/catalog/product). All the reagents were of analytical grade and used as received without further purification. Cyclic voltammetry (CV), and differential pulse voltammetry (DPV) were done on a CHI 900 (CH Instruments Company, made in the U.S.A) electrochemical workstation. Amperometric measurements were carried out on a CHI 1205B (CH Instruments Company, made in the U.S.A). The conventional three electrode system were used, a platinum wire as a counter electrode, a saturated Ag/AgCl electrode as the reference electrode and modified glassy carbon electrode (GCE) and unmodified GCE as the working electrode (GCE area: 0.071 cm^2 and rotating disk electrode (RDE) area: 0.2 cm^2 (rpm = 1400)). Electrochemical impedance measurements were taken from a IM6ex (ZAHNER elektrik) at a potential of 0.2 V (AC potential: 5 mV) within a frequency range of 0.01 to 100 kHz. The pH measurements were taken from a Clean pH meter (pH 500) with a combined pH glass electrode. The X-ray diffraction data were collected by using a XPERT-PRO diffractometer equipped with Cu Kα radiation (k = 1.54 Å). Fourier transform infrared (FT-IR) spectra were performed by a JASCO FT/IR-6600 spectrophotometer. The surface morphology was observed via transmission electron microscopy (TEM) on a TECNAI G^2 under an accelerating voltage of 200 kV.

Synthesis of g-C_3N_4/ZnO nanocomposite

The g-C_3N_4/ZnO nanocomposite were synthesized via a two-step self-assembly process. Herein, Nanorods-like ZnO was synthesized through a sonochemical method first. Briefly, the precursor solution of 0.5 g zinc acetate dihydrate was dissolved in 10 mL of DI water, followed by the drop wise addition of 0.1 M NaOH solution with continuous magnetic stirring. After that, 20 mL of methanol solution of ethylene diamine was added to the reaction mixture. The reaction mixture was ultrasonicated for 4 h. A milky white crystalline powder was collected through centrifugation (6000 rpm) and washed with DI water followed by ethanol. The crystalline powder was dried in a hot air oven at 100 °C for 12 h. The g-C_3N_4 support was prepared by a thermal polymerization of urea in air at 550 °C for 2 h. The g-C_3N_4 was grounded into fine powder, then adding 1 mg to 1 mL deionized water (DI) with the ultrasonic treatment for 30 min. Subsequently, different amount of ZnO nanorods were added into the above g-C_3N_4 suspension under ultrasound for 30 min. The resultant uniform suspension named as g-C_3N_4/ZnO nanocomposite and used for further characterization and electrochemical studies.

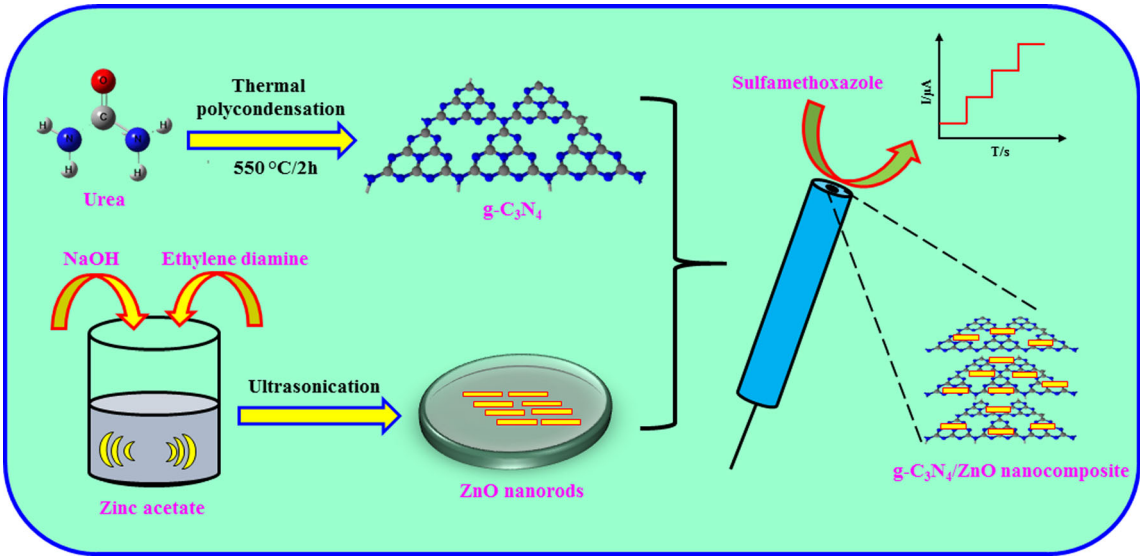

Scheme 1 Schematic representation of the present work

Fabrication of g-C_3N_4/ZnO nanocomposite modified electrode

Prior to use, glassy carbon electrode (GCE) was carefully polished to a mirror like plane with 0.5 and 0.05 mm alumina slurries, then cleaned ultrasonically in water and acetone, successively and dried at room temperature. Then, 6 μL (optimized) g-C_3N_4/ZnO nanocomposite colloid suspension was dropped on the pretreated GCE and allowed to dry at room temperature. Then, the electrode was rinsed thoroughly with deionized water to remove the physically adsorbed materials to form the g-C_3N_4/ZnO electrode for SMZ sensing. The modified electrodes were kept in room temperature, when not in use.

Results and discussions

Choice of material

Nowadays, the transition metal oxide (TMO) and g-C_3N_4 composite based-nanomaterials have gained considerable attention and are widely used in many fields [22, 24]. Several works proved that TMO/g-C_3N_4 based-nanomaterials owned the excellent catalysis efficiency in the field of electrochemical sensor [25, 26]. However, electrochemical sensing application of g-C_3N_4/ZnO is not reported. g-C_3N_4/ZnO already exhibited its excellent performances in the fields of photocatalysis, electrocatalysis, and gas sensor. In order to extend the great potential utilization of g-C_3N_4/ZnO, also to search the suit materials for the fabrication of electrochemical sensor, g-C_3N_4/ZnO nanocomposite was synthesized and utilized for electrochemical sensor.

Surface characterization

The phase structure of the g-C_3N_4 (a), ZnO (b) and g-C_3N_4/ZnO nanocomposite (c) were characterized by powder XRD, shown in Fig. 1a. According to the powder XRD data of g-C_3N_4 (a), two characteristic peaks is observed at 13.1 and 27.3°, perfectly indexed with as the (100) and (002) lattice plane of g-C_3N_4 [27], which were ascribed to in-plane structure packing unit and the interlayer staking. The XRD pattern of ZnO (b) and g-C_3N_4/ZnO nanocomposite (c) displays the diffraction peaks at 31.9, 34.5, 36.4, 47.6, 56.6, 62.9, 66.5, 68.1 and 69.2° which were attributed to the (100), (002), (101), (102), (110), (103), (200), (112) and (201) crystal planes of hexagonal Wurtzite structure of ZnO (JCPDS Card No. 36–1451) [28]. The presence of g-C_3N_4 diffraction peak at 2θ of 13.1 and 27.3° confirms the composite structure of the g-C_3N_4/ZnO sample (c).

Figure 1b shows the FT-IR spectra of g-C_3N_4 (a), ZnO (b), and g-C_3N_4/ZnO nanocomposite (c). Typical spectrum of g-C_3N_4 shows the peaks at 805 cm^{-1} is assigned to the characteristic vibration mode of triazine ring system [22]. The broad band appeared at 3200 cm^{-1} due to the vibration of primary and secondary amine [27]. The peaks in the range of 1300–1650 cm^{-1} several strong bands are observed, which are likely due to heptazine-derived repeating units [29]. FT-IR spectrum of ZnO (b) shows characteristic bands at 430 and 3450 cm^{-1}, correspond to Zn–O bond vibration and –OH stretching vibrations, respectively [28]. The FTIR spectrum of g-C_3N_4/ZnO nanocomposite (c) exhibited the corresponding characteristic peaks of g-C_3N_4 (a) and ZnO (b), authenticates the successful formation of g-C_3N_4/ZnO nanocomposite. The peak observed at 430 cm^{-1} of ZnO (b) shifted to 470 cm^{-1}

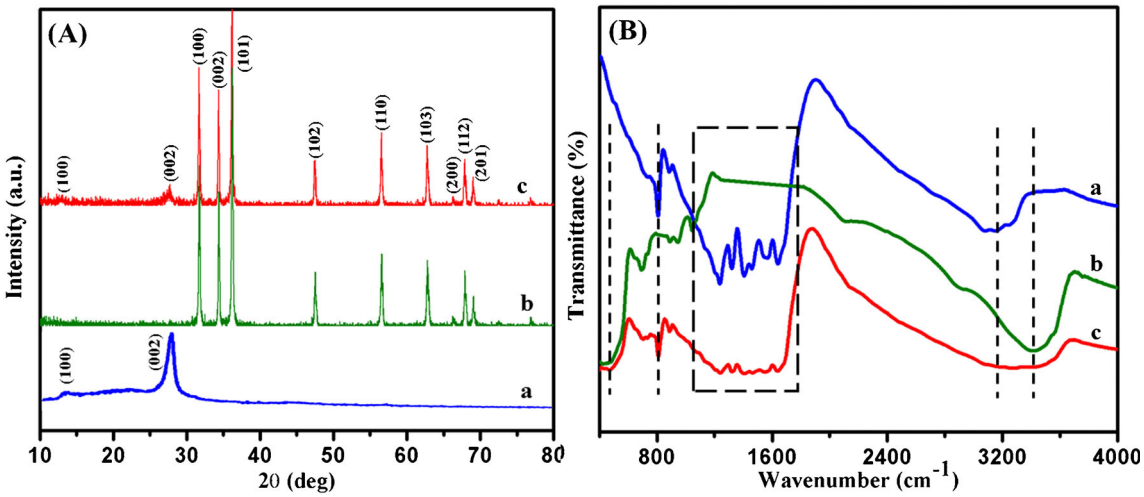

Fig. 1 **a** XRD patterns of g-C_3N_4 (a), ZnO (b), and g-C_3N_4/ZnO nanocomposite (c). **b** FT-IR spectrum of g-C_3N_4 (a), ZnO (b), and g-C_3N_4/ZnO nanocomposite (c)

in the case of g-C_3N_4/ZnO nanocomposite (c), suggest that the triazine rings of g-C_3N_4 are successfully interact with ZnO via electrostatic interaction. These results confirmed the formation of g-C_3N_4/ZnO nanocomposite.

The morphologies and structure of the g-C_3N_4/ZnO nanocomposite were evaluated by FESEM and TEM and shown in Fig. 2. Figure 2a and b shows the FESEM images of the g-C_3N_4/ZnO nanocomposite, it can be seen that the smooth ZnO nanorods were uniformly dispersed onto the g-C_3N_4 sheets. The HRTEM image were shown in Fig. 2d, corresponding to the red framed area in Fig. 2c. The enlarged high resolution TEM (Fig. 2d) shows that the crystal planes are (002) planes with lattice fringes with a spacing of 0.26 nm. Figure 2d inset shows the FFT pattern of the corresponding HRTEM, which are consistent with XRD patterns.

Electrochemical impedance spectroscopy (EIS) and electrode kinetics

Fig. S2A. displays the impedance curve (Nyquist plots) of bare GCE (a), ZnO/GCE (b), g-C_3N_4/GCE (c) and g-C_3N_4/ZnO/GCE (d) under open-circuit potential condition using 0.1 M KCl solution containing 5 mM $Fe(CN)_6^{3-/4-}$ (1:1) at a frequency range from 0.01 to 100 kHz. In Nyquist plots, diameter of the semicircle in terms of frequency corresponds to the electron-transfer in the limiting process, in other words electron transfer resistance (Rct), and the straight line at the low frequency corresponds to the dispersion process. It can be seen from Fig. S2A that the g-C_3N_4/ZnO/GCE (d) exhibited a very small semicircle domain (32 Ω), implying very low electron transfer resistance (Rct) is lower than that of the bare GCE (366 Ω), ZnO/GCE (135 Ω), and g-C_3N_4/GCE (89 Ω). This is attributed to the excellent electronic conductivity and rapid electron transfer of the g-C_3N_4/ZnO nanocomposite.

The peak potential separation (ΔEp) and active surface area of g-C_3N_4/ZnO/GCE were studied by using CV technique based on the electrochemical redox process of ferricyanide system. Fig. S2B shows the recorded CV curve of modified electrodes such as bare GCE (a), ZnO/GCE (b), g-C_3N_4/GCE (c) and g-C_3N_4/ZnO/GCE (d) in 5 mM of $[Fe(CN)_6]^{3-/4-}$ containing 0.1 M of KCl, where the scan rate is fixed to be 50 mV s^{-1}. The result clearly shows that the g-C_3N_4/ZnO/GCE exhibited the highest redox peak current response (Ipa = −132.3 μA and Ipc = 138.2 μA) with lowest peak potential separation (ΔEp = 0.089 V). Whereas, the redox peak current and ΔEp were measured for g-C_3N_4/GCE (c) (Ipa = −121.2 μA and Ipc = 124.1 μA, ΔEp = 0.093 V), ZnO/GCE (b) (Ipa = −105.5 μA and Ipc = 111.3 μA, ΔEp = 0.096 V) and bare GCE (a) (Ipa = −102.9 μA and Ipc = 102.7 μA, ΔEp = 0.099 V). The highest redox current response with lowest peak potential separation facilitates the fast electron transfer towards the electrode in bulk solution. In order to detect the active surface area of the modified electrodes, the CV curve of g-C_3N_4/ZnO/GCE was recorded by varying the applied scan rate from 20 to 200 mV s^{-1} in the similar working condition as followed in Fig. S2B. The resultant CV curve is shown in Fig. S2C with linearly increasing redox peak current for increasing scan rate. The linear relationship between redox peak current and square root of scan rate is clearly demonstrated in the linear calibration plot (Fig. S2D) with detected linear regression equation (Ipa (μA) = −20.43 $(v^{1/2}(mV\ s^{-1})^{1/2})$ +31.4, $R^2 = 0.9999$ and Ipc = 18.17 $(v^{1/2}(mV\ s^{-1})^{1/2})$ +13.54, $R^2 = 0.9997$). It is exhibiting that the overall electrochemical redox reaction of ferricyanide system is following the diffusion controlled process.

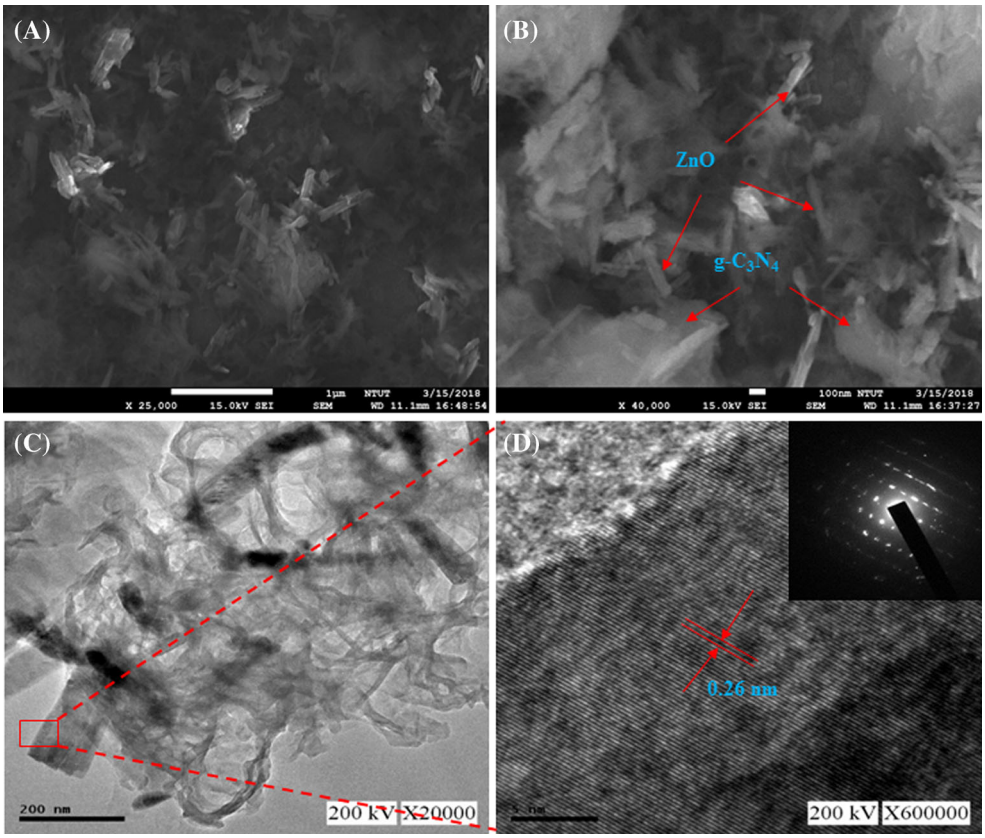

Fig. 2 FESEM image of g-C_3N_4/ZnO nanocomposite (**a** and **b**). TEM image (**c**) and HRTEM image (**d**) of g-C_3N_4/ZnO nanocomposite

The active surface area of modified electrodes was detected by using the Randles-Sevick equation [30].

$$Ip = 2.69 \times 10^5 AD^{1/2} n^{3/2} \nu^{1/2} C \quad (1)$$

Where Ip represents the peak current, A is the active surface area, D is referred as the diffusion coefficient of ferricyanide solution, n is represented the number of electron transfer ($n = 1$), ν is the applied scan rate (V s^{-1}) and, C is the concentration of ferricyanide ($[Fe(CN)_6]^{3-/4-}$) in bulk solution. By following the above Eq. (1), the value of A was detected to be 0.1236 cm^2 for g-C_3N_4/ZnO/GCE. While, the value of A for g-C_3N_4/GCE, ZnO/GCE and bare GCE, were detected to be 0.1058, 0. 094 and 0.08 cm^2, respectively.

Consequently, the charge transfer rate (ks) of all modified electrodes were detected based on Rct by using the Eq. (2) [31],

$$Rct = RT/n^2 F^2 Cks \quad (2)$$

Where, R is the gas constant (8.314 J mol^{-1} K^{-1}) represents which is accordance with the previously reported literature the peak current, T is the room temperature (298 K), n is the number of electrons involved, F is the Faraday constant (96,485 C/mol), A is the active surface area (cm^2), C is referred as the concentration of ferricyanide ($[Fe(CN)_6]^{3-/4-}$) in bulk solution. By using the above Eq. (2), the ks was measured for bare GCE (a), ZnO/GCE (b), g-C_3N_4/GCE (c) and g-C_3N_4/ZnO/GCE (d) to 1.46×10^{-7}, 3.94×10^{-7}, 5.98×10^{-7}, 1.66×10^{-6} cm s^{-1}, respectively.

Electrochemical behavior of differently modified electrodes

Figure 3a displays the electrochemical behavior of 500 μM SMZ on the bare GCE (a), ZnO/GCE (b), g-C_3N_4/GCE (c) and g-C_3N_4/ZnO/GCE (d) investigated by CV in 0.05 M phosphate buffer (pH 7.0) at a scan rate of 50 mV s^{-1}. As shown in Fig. 3a, the bare GCE (a) exhibits negligible catalytic effects on SMZ electro-oxidation. In the case of ZnO/GCE a small current response (146.84 μA cm^{-2}) was observed at 0.95 V (E_{pa}), whereas the anodic current response of g-C_3N_4/GCE (c) slightly increased (181.23 μA cm^{-2}), indicate that pure ZnO and g-C_3N_4 slightly improve sensing of SMZ compared with bare electrode. However, g-C_3N_4/ZnO/GCE shows a well-defined, sharp oxide-current peak (E_{pa} = 0.88 V) with enhanced anodic peak current density (248.54 μA cm^{-2}) towards SMZ oxidation. This is attributed to the excellent electronic conductivity, and a great synergetic effect of g-C_3N_4/ZnO/GCE. It is clear that the change of the CV response is consistent with impedance and active surface area studies.

Effect of pH value and scan rate

Fig. S4 shows the CVs of 500 μM SMZ onto g-C_3N_4/ZnO/GCE in phosphate buffers of different pH values (3.0, 5.0, 7.0,

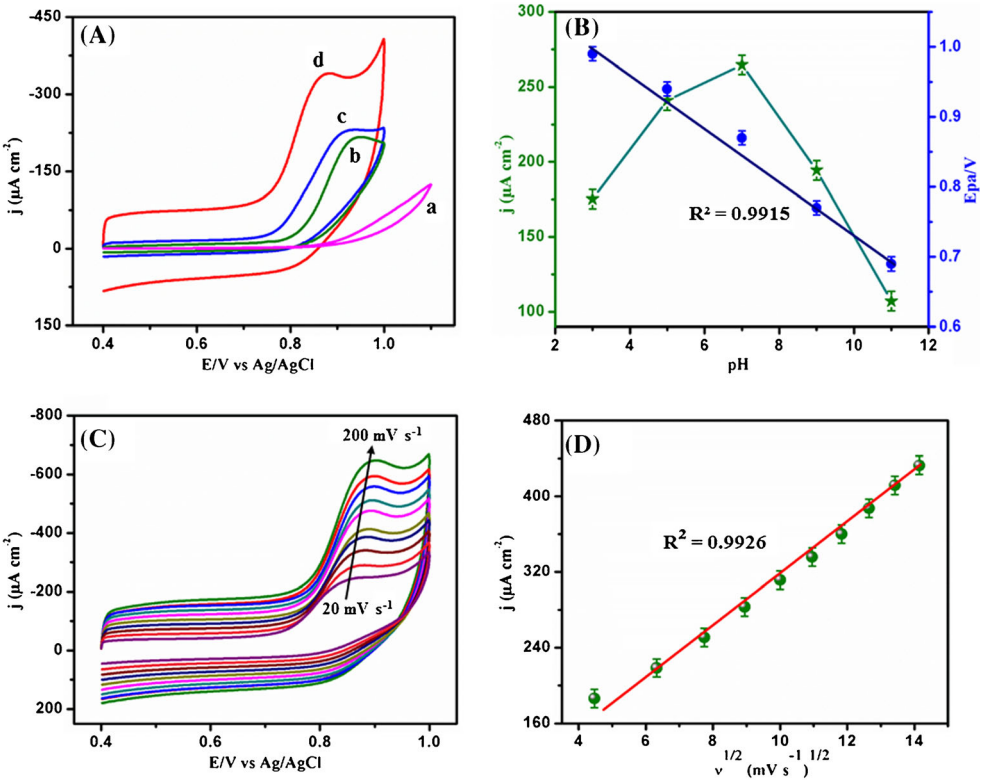

Fig. 3 CVs of bare GCE (**a**), ZnO/GCE (**b**), g-C_3N_4/GCE (**c**), and g-C_3N_4/ZnO/GCE (**d**) in phosphate buffer (pH 7.0) containing 500 μM SMZ at a scan rate of 50 mV s^{-1}. **b** pH vs anodic peak current (I_{pa}) (green) and calibration plot for pH vs anodic peak potential (E_{pa}) (blue). (C) CVs for g-C_3N_4/ZnO/GCE in phosphate buffer (pH 7.0) containing 500 μM of SMZ at different sweep rates (20–200 mV s^{-1}). (D) Calibration plot of square root of scan rate ($\nu^{1/2}$) vs anodic peak current (I_{pa}) of SMZ

9.0, and 11.0) at a scan rate of 50 mV s^{-1}. It can be seen that the increasing solution pH, the anodic peak potential (E_{pa}) gradually shifted towards less positive potential values as well as rise in the peak current was observed and utmost current response was attained at pH 7.0. The results shows that the oxidation peak potential and current were strongly influenced by solution pH. Considering the sensitivity, pH 7 was chosen as an optimized buffer for further electrochemical experiments. The effect of pH on the oxidation peak potential (E_{pa}) for SMZ oxidation shown in Fig. 3b (blue). The linear relationship between E_{pa} and pH can be written as, Ep = −0.0575 pH + 1.1195, with a correlation coefficient of 0.9915. The slope value of dE_{pa}/dpH (0.0575 V/pH) indicates that the equal number of proton and electrons involved in the oxidation of SMZ [11], this is consistent with previous reports.

The effect of scan rates upon the electrochemical oxidation behavior of SMZ was studied in phosphate buffer pH 7.0 at different scan rates in the range of 20–200 mV s^{-1}, which is depicts in Fig. 3c. As the scan rate increases, the corresponding oxidation current increases along with a gradual potential shift of the oxidation potential towards positive direction. It can be found in the Fig. 3d, the anodic peak current linearly proportional to the square root of the scan rates with a correlation coefficient of 0.9926, such dependence indicates that the oxidation of SMZ is a typical diffusion controlled and this is consistent with previous studies [1].

Analytical performance

Amperometric measurements were carried out at +0.88 V on g-C_3N_4/ZnO modified RDE by successive injection of SMZ (Fig. 4a) into phosphate buffer (pH 7.0) under stirring. As can be seen in Fig. 4a, the g-C_3N_4/ZnO/RDE achieves 96% of the steady state current within 4 s after the injection of SMZ, indicating a rapid and higher electron exchange between SMZ and electrode. As the intensity of oxidation increases significantly with the increase of SMZ concentration. The corresponding current-concentration calibration plot in Fig. 4b clearly shows that the linear regression equation, I_{pa} (μA) = 2.8179 + 0.449 [SMZ] (μM), with R^2 = 0.9942. The sensor demonstrates a linear range of 0.02–1105 μM a response sensitivity of 3.18 μA μM^{-1} cm^{-2}. The limit of detection (LOD) was calculated by IUPAC method as shown below:

$$LOD = 3\sigma/m$$

Here, σ is the standard deviation of the blank and m is the slope of the calibration plot. The LOD of the sensor was determined to be 6.6 nM. The LOD values and linear ranges for SMZ detection were compared with those from previous work performed with different electrode materials, summarized in Table 1. It is worth mentioning that g-C_3N_4/ZnO modified electrode exhibits satisfactory

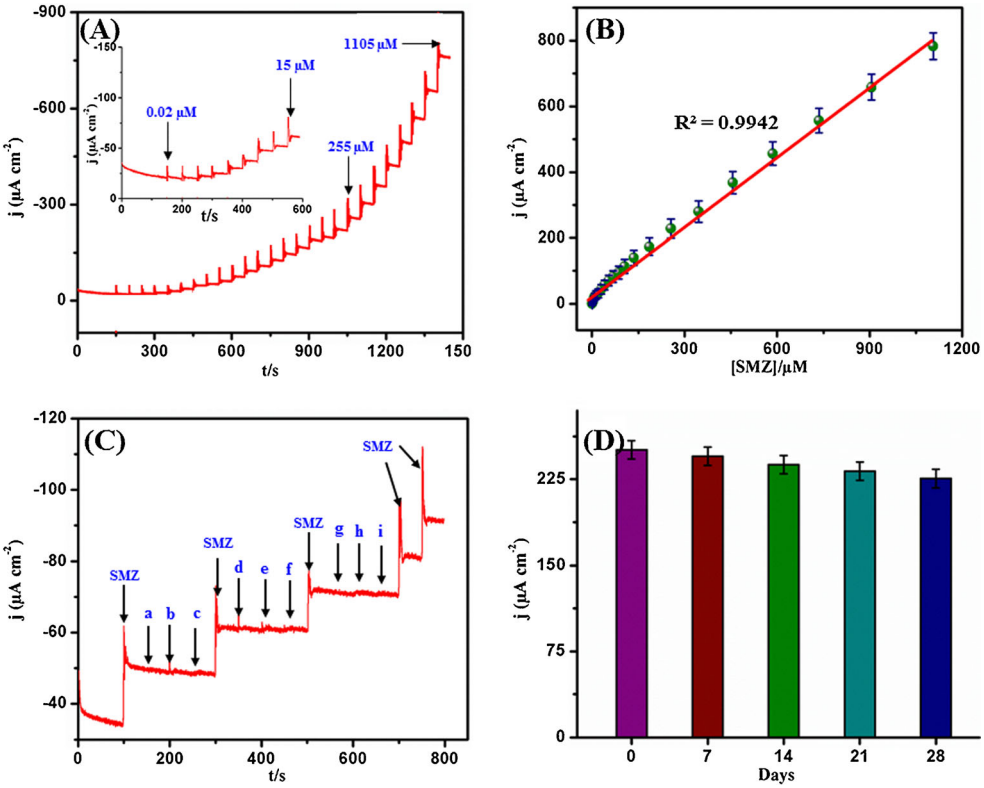

Fig. 4 **a** Amperometric current response of g-C_3N_4/ZnO modified RDE upon the successive addition of different amount of SMZ into phosphate buffer (pH 7.0). **b** The calibration plot of [SMZ] vs current density (j). **c** Amperometric current response of g-C_3N_4/ZnO/RDE to successive injection of SMZ and other interferents including ascorbic acid (a), uric acid (b), dopamine (c), trimethoprim (d), phenazopyridine (e) sulfadiazine (f), sulfamethizole (g), glucose (h) and H_2O_2 (i). **d** Current response of g-C_3N_4/ZnO/GCE for 500 μM SMZ in different time periods

integrative performance with very high sensitivity and lowest LOD (6.6 nM) when compared with that from previous works. Fig. S5A shows the DPV response of g-C_3N_4/ZnO modified electrode for different SMZ concentrations. The SMZ peak current increased linearly at 0.02–623 μM. As shown in Fig. S5B, a good correlation coefficient ($R^2 = 0.9985$) was found among the SMZ concentration and peak current. The calculated limit of detection to be 5.78 nM, consistent with amperometric measurements. The above results can be attributed to the higher electronic conductivity and excellent synergistic effect of g-C_3N_4/ZnO nanocomposite.

Table 1 Comparison of the analytical performance of the sensor with previously reported SMZ sensors

Electrode material	Linear range (μM)	LOD (μM)	ref
FeZnO/CPE	2–160	0.03	[2]
HT-BDD	–	0.0144	[3]
NiO/GO/CPE	0.08–550	0.04	[9]
p-DAN/GCE	0.5–150	0.05	[11]
TYR-AuNPs-SPCEs	20–200	22.6 ± 2.1	[14]
BDD	6.1–60.1	1.15	[32]
MWCNT/PBnc/SPE	1.0–10.0	0.038	[33]
MIP/BDD	0.1–100	0.0241	[4]
MWCNT/GCE	50–1000	10	[13]
g-C_3N_4/ZnO/GCE	0.02–1105	0.0066	This work

Selectivity, reproducibility and stability

To examine the selectivity of the g-C_3N_4/ZnO modified electrode was tested by succession injection of 100 μM SMZ and 500 μM of interfering compounds into phosphate buffer at an applied potential +0.88 V. It can be observed that, after the injection of 100 μM SMZ, the current apparently increases, while no distinctive current change can be observed after the injection of ascorbic acid (a), uric acid (b), dopamine (c), trimethoprim (d), phenazopyridine (e) sulfadiazine (f), sulfamethizole (g), glucose (h) and H_2O_2 (i) (Fig. 4c); thus, a good selectivity has been demonstrated. This selectivity may be due to the hydrogen bonding interaction existing between the amine group (-NH_2) of target molecule and the negatively charged N atom of g-C_3N_4. The feasible selectivity comes from the distribution of electron charges in the investigated target analyte and interference molecules is not uniform in the particular positions, due to the presence of various functional groups. The energy of the highest filled orbital only determines the ease of giving up electrons and indicates the active site that is most susceptible to the oxidation reaction. Thus, g-C_3N_4/ZnO based sensor has high selectivity toward SMZ sensing.

The reproducibility of the sensor was examined by measuring the current response of SMZ oxidation at five equally fabricated electrodes under the same conditions. The relative standard deviation of the current response was 2.3% indicating the sensor is highly reproducible. Furthermore,

five successive measurements on each sensor gave a RSD of about 2.1–2.6%. The sensor is stored in a desiccator at ambient conditions and measure 500 μM SMZ every one week. The results (Fig. 4d) shows there is no significant decrease of the current response after one week, and only 2.4% decrease after 4 weeks. This long-term stability of the sensor can be attributed to the excellent chemical stability of the g-C_3N_4/ZnO nanocomposite.

Detection of SMZ in physiological samples

The sensor was applied to a SMZ assay with standard human blood serum samples by adding different concentrations of SMZ using standard addition method. The blood serum samples was used as a real sample and spiked with the known concentration of SMZ. Consequently, the amperometric experiment was performed in pH 7 phosphate buffer at a fixed potential of +0.88 V by using the SMZ spiked blood serum sample and tested for n times ($n = 3$). The average percent recovery, including RSD, was calculated from three samples, as listed in Table S1. As shown in Table S1, spike recoveries of SMZ from three samples were found to be 99.8, 99.6, and 100.1% and relative standard deviations were less than 3% for three independent measurements. All these observations suggest that the SMZ sensor is promising for SMZ detection with satisfactory reliability in actual implementation.

Conclusion

A super-sensitive and selective electrochemical sensing platform for detecting SMZ based on g-C_3N_4/ZnO nanocomposite modified GCE is reported. The Nanorod architecture provided large accessible area of ZnO active sites with facilitated ion transfer, while the interconnected g-C_3N_4 nanosheets offered continuous electron pathways for efficient electroactive ZnO. The experiment results show that the g-C_3N_4/ZnO based sensor exhibits higher electron transfer rate ($ks = 1.66 \times 10^{-6}$ cm s^{-1}) and large active surface (0.1236 cm^2). The g-C_3N_4/ZnO nanocomposite modified electrode displays distinctly enhanced electrocatalytic activity towards the oxidation of SMZ. Furthermore, g-C_3N_4/ZnO modified electrode exhibited a reasonable selectivity against various interference and good reproducibility towards the detection of SMZ. The g-C_3N_4/ZnO was also applied to the detection of SMZ content human blood serum sample in with satisfactory results, and the sensor can keep its activity for at least 4 weeks. All these features indicate that the g-C_3N_4/ZnO nanocomposite is a promising material in the field of biosensor.

Acknowledgements The authors gratefully acknowledge the financial support of the Ministry of Science and Technology, Taiwan through contract no. MOST 106-2113-M-027-003.

Compliance with ethical standards The author(s) declare that they have no competing interests.

References

1. Arvand M, Ansari R, Heydari L (2011) Electrocatalytic oxidation and differential pulse voltammetric determination of sulfamethoxazole using carbon nanotube paste electrode. Mater Sci Eng C 31: 1819–1825
2. Meshki M, Behpour M, Masoum S (2015) Application of Fe doped ZnO nanorods-based modified sensor for determination of sulfamethoxazole and sulfamethizole using chemometric methods in voltammetric studies. J Electroanal Chem 740:1–7
3. Andrade LS, Rocha-Filho RC, Cass QB, Fatibello-Filho O (2009) Simultaneous differential pulse voltammetric determination of sulfamethoxazole and trimethoprim on a boron-doped diamond electrode. Electroanalysis 21:1475–1480
4. Zhao Y, Yuan F, Quan X, Yu H, Chen S, Zhao H, Liu Z, Hilal N (2015) An electrochemical sensor for selective determination of sulfamethoxazole in surface water using a molecularly imprinted polymer modified BDD electrode. Anal Methods 7:2693–2698
5. Nagaraja P, Naik SD, Shreshta AK, Shivakumar A (2007) A sensitive spectrophotometric method for the determination of sulfonamides in pharmaceutical preparations. Acta Pharma 57:333–342
6. Chiavarino B, Crestoni ME, Marzio AD, Fornarini S (1998) Determination of sulfonamide antibiotics by gas chromatography coupled with atomic emission detection. J Chromatogr Biomed Appl 706:269–277
7. Weber A, Opheim KE, Siber GR, Ericson JF, Smith AL (1983) High-performance liquid chromatographic quantitation of trimethoprim, sulfamethoxazole, and N4-acetylsulfamethoxazole in body fluids. J Chromatogr 278:337–345
8. You T, Yang X, Wang E (1998) Determination of sulfadiazine and sulfamethoxazole by capillary electrophoresis with end-column electrochemical detection. Analyst 123:2357–2360
9. Shabani-Nooshabadi M, Roostaee M (2016) Modification of carbon paste electrode with NiO/graphene oxide nanocomposite and ionic liquids for fabrication of high sensitive voltammetric sensor on sulfamethoxazole analysis. J Mol Liq 220:329–333
10. Balasubramanian P, Balamurugan TST, Chen SM, Chen TW (2017) Facile synthesis of orthorhombic strontium copper oxide microflowers for highly sensitive nonenzymatic detection of glucose in human blood. J Taiwan Inst Chem Eng 81:182–189
11. Chasta H, Goyal RN (2015) A simple and sensitive Poly-1,5-Diaminonaphthalene modified sensor for the determination of Sulfamethoxazole in biological samples. Electroanalysis 27: 1229–1237
12. Cesarino I, Cesarino V, Lanza MR (2013) Carbon nanotubes modified with antimony nanoparticles in a paraffin composite electrode: simultaneous determination of sulfamethoxazole and trimethoprim. Sensors Actuators B Chem 188:1293–1299
13. Issac S, Girish Kumar K (2009) Voltammetric determination of sulfamethoxazole at a multiwalled carbon nanotube modified glassy carbon sensor and its application studies. Drug Test Anal 1:350–354
14. del Torno-de Román L, Alonso-Lomillo MA, Domínguez-Renedo O, Arcos-Martínez MJ (2016) Tyrosinase based biosensor for the electrochemical determination of sulfamethoxazole. Sensors Actuators B Chem 227:48–53

15. Liu B, Liu G, Xiao B, Yan J (2018) Molecularly imprinted electrochemical sensor for the determination of Sulfamethoxazole. J New Mater Electrochem Syst 21:077–080
16. Ding J, Zhu S, Zhu T, Sun W, Li Q, Wei G, Su Z (2015) Hydrothermal synthesis of zinc oxide-reduced graphene oxide nanocomposites for an electrochemical hydrazine sensor. RSC Adv 5:22935–22942
17. Wang Y, Wang S, Tao L, Min Q, Xiang J, Wang Q, Xie J, Yue Y, Wu S, Li X, Ding H (2015) A disposable electrochemical sensor for simultaneous determination of norepinephrine and serotonin in rat cerebrospinal fluid based on MWNTs-ZnO/chitosan composites modified screen-printed electrode. Biosens Bioelectron 65:31–38
18. Ameen S, Akhtar MS, Shin HS (2012) Highly sensitive hydrazine chemical sensor fabricated by modified electrode of vertically aligned zinc oxide nanorods. Talanta 100:377–383
19. Palanisamy S, Chen SM, Sarawathi R (2012) A novel nonenzymatic hydrogen peroxide sensor based on reduced graphene oxide/ZnO composite modified electrode. Sens Actuators B Chem 166:372–377
20. Selvarajan S, Suganthi A, Rajarajan M (2018) Fabrication of g-C_3N_4/NiO heterostructured nanocomposite modified glassy carbon electrode for quercetin biosensor. Ultrason Sonochem 41:651–660
21. Lv H, Ji G, Yang Z, Liu Y, Zhang X, Liu W, Zhang H (2015) Enhancement photocatalytic activity of the graphite-like C_3N_4 coated hollow pencil-like ZnO. J Colloid Interface Sci 450:381–387
22. Wang J, Yang Z, Gao X, Yao W, Wei W, Chen X, Zong R, Zhu Y (2017) Core-shell g-C_3N_4@ZnO composites as photoanodes with double synergistic effects for enhanced visible-light photoelectrocatalytic activities. Appl Catal B 217:169–180
23. Sadhukhan M, Barman S (2013) Bottom-up fabrication of two-dimensional carbon nitride and highly sensitive electrochemical sensors for mercuric ions. J Mater Chem A 1:2752–2756
24. Liu W, Wang M, Xu C, Chen S (2012) Facile synthesis of g-C_3N_4/ZnO composite with enhanced visible light photooxidation and photoreduction properties. Chem Eng J 209:386–393
25. Zou J, Wu S, Liu Y, Sun Y, Cao Y, Hsu JP, Wee ATS, Jiang J (2018) An ultra-sensitive electrochemical sensor based on 2D g-C_3N_4/CuO nanocomposites for dopamine detection. Carbon 130:652–663
26. Liu L, Wang MD, Wang CY (2018) In-situ synthesis of graphitic carbon nitride/iron oxide-copper composites and their application in the electrochemical detection of glucose. Electrochim Acta 265:275–283
27. Balasubramanian P, Balamurugan TST, Chen SM, Chen TW, Ali MA, Al-Hemaid FM, Elshikh MS (2018) An Amperometric sensor for low level detection of antidepressant drug carbamazepine based on Graphene oxide-g-C_3N_4 composite film modified electrode. J Electrochem Soc 165:B160–B166
28. Thirumalraj B, Rajkumar C, Chen SM, Lin KY (2017) Determination of 4-nitrophenol in water by use of a screen-printed carbon electrode modified with chitosan-crafted ZnO nanoneedles. J Colloid Interface Sci 499:83–92
29. Wang G, Kuang S, Zhang J, Hou S, Nian S (2016) Graphitic carbon nitride/multiwalled carbon nanotubes composite as Pt-free counter electrode for high-efficiency dye-sensitized solar cells. Electrochim Acta 187:243–248
30. Balasubramanian P, Settu R, Chen SM, Chen TW, Sharmila G (2018) A new electrochemical sensor for highly sensitive and selective detection of nitrite in food samples based on sonochemical synthesized calcium ferrite ($CaFe_2O_4$) clusters modified screen printed carbon electrode. J Colloid Interface Sci 524:417–426
31. Sukanya R, Sakthivel M, Chen SM, Chen TW (2018) A new type of terbium diselenide nano octagon integrated oxidized carbon nanofiber: an efficient electrode material for electrochemical detection of morin in the food sample. Sensors Actuators B Chem 269:354–367
32. Souza CD, Braga OC, Vieira IC, Spinelli A (2008) Electroanalytical determination of sulfadiazine and sulfamethoxazole in pharmaceuticals using a boron-doped diamond electrode. Sensors Actuators B Chem 135:66–73
33. Sgobbi LF, Razzino CA, Machado SA (2016) A disposable electrochemical sensor for simultaneous detection of sulfamethoxazole and trimethoprim antibiotics in urine based on multiwalled nanotubes decorated with Prussian blue nanocubes modified screen-printed electrode. Electrochim Acta 191:1010–1017